THE JOURNAL OF PHYSICAL CHEMISTRY Letters

Letter

Cite This: J. Phys. Chem. Lett. 2018, 9, 513−520

pubs.acs.org/JPCL

Energetic Costs, Precision, and Transport Efficiency of Molecular Motors

Wonseok Hwang and Changbong Hyeon*

Korea Institute for Advanced Study, Seoul 02455, Republic of Korea

Supporting Information

ABSTRACT: An efficient molecular motor would deliver cargo to the target site at a high speed and in a punctual manner while consuming a minimal amount of energy. According to a recently formulated thermodynamic principle, referred to as the *thermodynamic uncertainty relation*, the travel distance of a motor and its variance are, however, constrained by the free energy being consumed. Here we use the principle underlying the uncertainty relation to quantify the *transport efficiency* of molecular motors for varying ATP concentration ([ATP]) and applied load (f). Our analyses of experimental data find that transport efficiencies of the motors studied here are semioptimized under the cellular condition. The efficiency is significantly deteriorated for a kinesin-1 mutant that has a longer neck-linker, which underscores the importance of molecular structure. It is remarkable to recognize that, among many possible directions for optimization, biological motors have evolved to optimize the transport efficiency in particular.

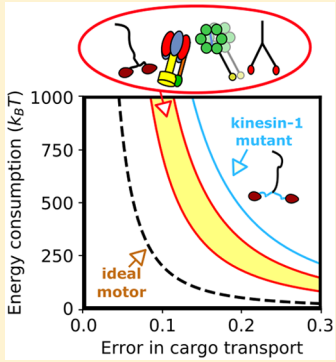

Biological systems function in nonequilibrium steady states (NESS) where the energy and material currents flow constantly in and out of the system. Subjected to incessant thermal and nonequilibrium fluctuations, cellular processes are inherently stochastic and error-prone. Thus, biological systems adopt a plethora of error-correcting mechanisms that expend energy to fix any error deleterious to their functions. Trade-off relations between the energetic cost and information processing are ubiquitous in cellular processes and have been a recurring theme for many decades.[1−7]

A recent study by Barato and Seifert[8] has formulated the *thermodynamic uncertainty relation*, which quantifies the trade-off between free energy consumption and precision of a dynamic process in NESS. They defined the uncertainty measure $\mathcal{Q}$, a product between the energy consumption ($Q(t)$) of the process and the squared relative error of an output observable from the process $X(t)$, $\epsilon_X^2(t) = \langle \delta X^2 \rangle / \langle X \rangle^2$, and further conjectured that $\mathcal{Q}$ cannot be smaller than $2k_BT$ for any chemical network described by Markov jump processes, which is succinctly written as

$$\mathcal{Q} = Q(t) \times \epsilon_X^2(t) \geq 2k_BT \tag{1}$$

The measure $\mathcal{Q}$ quantifies the uncertainty of the dynamic process. The proof and physical significance of this inequality have been discussed extensively.[8−13] Among others, we have shown that the minimal bound of $\mathcal{Q}$, $2k_BT$, is attained when heat dissipated from the process is normally distributed, such that $P(Q) \approx e^{-Q^2}$, which is realized in special conditions.[12] In the presence of large fluctuations inherent to cellular processes, harnessing energy into precise motion and suppressing the uncertainty are critical for accuracy in cellular computation. The smaller the value of $\mathcal{Q}$, the more regular and predictable the trajectory generated from the process.

Historically, the efficiency of the heat engine has been assessed in terms of maximizing the amount of work or power extracted from two heat reservoirs with different temperatures.[14−16] In contrast to the heat engine, molecular motors function at isothermal condition. Instead of a heat source, chemical forces that are constantly regulated in the live cell drive the molecules. While there are a number of different ways to assess the "thermodynamic efficiency" of a molecular motor,[17−20] another type of efficiency, which is more relevant for the function of the molecular motor, can be proposed. The uncertainty measure $\mathcal{Q}$ can be used to assess the efficiency of suppressing the uncertainty in dynamical processes by means of energy consumption and thus is quite pertinent for evaluating the *transport efficiency* of a motor (or motors).[21] The connection between $\mathcal{Q}$ and the transport efficiency becomes clear by recasting eq 1 into

$$\mathcal{Q} = \dot{Q}\frac{2D}{V^2} \geq 2k_BT \tag{2}$$

where we selected the displacement (or travel distance) of a motor as an output observable, substituting $X = l(t)$ into eq 1. $\mathcal{Q}$ is minimized by a motor that transports cargo (i) at a high speed ($V \approx \langle l(t) \rangle / t$), (ii) with a small error ($D \approx \langle \delta l(t)^2 \rangle / t$) in the displacement (or punctual delivery to a target site), and (iii) with a small energy consumption ($\dot{Q}$). Thus, a motor efficient in cargo transport is characterized by a small $\mathcal{Q}$ with its minimal bound $2k_BT$.

Received: December 3, 2017
Accepted: January 12, 2018
Published: January 12, 2018

DOI: 10.1021/acs.jpclett.7b03197
J. Phys. Chem. Lett. 2018, 9, 513−520

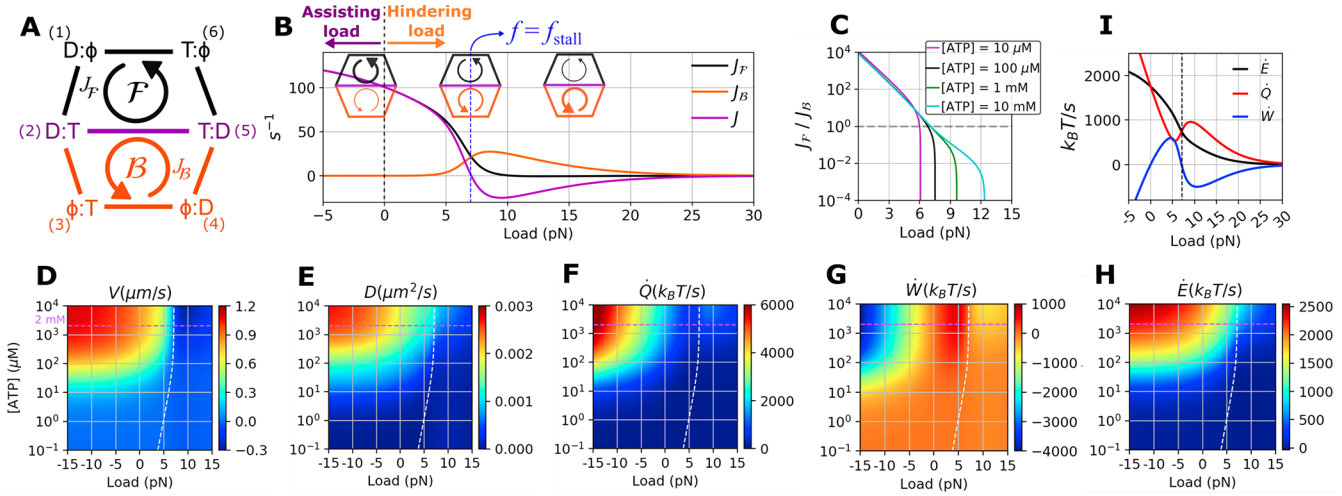

Figure 1. Dynamics of kinesin-1 generated from the six-state double-cycle kinetic network model. (A) Schematics of the network model for the hand-over-hand dynamics of kinesin-1, where T, D, and ϕ denote ATP-, ADP-bound, and apo states, respectively. Through ATP binding [(1) → (2)], mechanical step [(2) → (5)], release of ADP [(5) → (6)], and hydrolysis of ATP [(6) → (1)], kinesin moves forward in the $\mathcal{F}$ cycle [(1) → (2) → (5) → (6) → (1)] and backward in the $\mathcal{B}$ cycle [(4) → (5) → (2) → (3) → (4)]. The arrows in the figure depict the direction of reaction currents. In both cycles, each chemical step is reversible and the transition rate from the ith to jth state is given by k_{ij}. (B) Reaction current $J_{\mathcal{F}}$, $J_{\mathcal{B}}$, and J as a function of load. The three cartoons illustrate the amount of current along the $\mathcal{F}$ and $\mathcal{B}$ cycles as a function of f. $f < 0$ and $f > 0$ correspond to the assisting and hindering loads, respectively. (C) Ratio between the forward and backward fluxes ($J_{\mathcal{F}}/J_{\mathcal{B}}$) as a function of f at fixed [ATP]. The stall forces, determined at $J_{\mathcal{F}}/J_{\mathcal{B}} = 1$ (dashed line), are narrowly distributed within f = 6−8 pN. (D−H) V, D, $\dot{Q}$, $\dot{W}$, and $\dot{E}$ as a function of f and [ATP]. The white dashed lines demarcate the locus of the [ATP]-dependent stall force, and the dashed lines in magenta indicate the condition of [ATP] = 2 mM. (I) Dependences of $\dot{E}$, $\dot{Q}$, and $\dot{W}$ on f at [ATP] = 2 mM.

Here, we assess the "transport efficiency" of several biological motors using $\mathcal{Q}$ and study how it changes with varying conditions of f and [ATP]. To evaluate $\mathcal{Q}$, one should know $\dot{Q}$, D, and V of the system (see eq 2), which can be obtained by considering a suitable kinetic model that delineates the dynamical characteristics of the system.[22] Of particular interest is identifying a condition, if any, when the transport efficiency of a motor is optimized. Our analyses of motors show that the structure of $\mathcal{Q}(f, [\mathrm{ATP}])$ is sensitive to the design of the motor structure as well as the motor type. The biological motors studied here are semioptimized in terms of $\mathcal{Q}$ under the cellular condition, which alludes to the role of evolutionary pressure that has shaped the present forms of molecular motors in the cell.

Chemical Driving Force, Reaction Current, Work, and Heat Production Associated with the Dynamics of Kinesin-1 Using the Double-Cycle Network Model. To study the transport property of a molecular motor, we construct a suitable kinetic network model of the motor and compare the analytic expression of V and D in terms of a set of kinetic rates ($\{k_{ij}\}$) with the experimental data of V and D obtained at varying f and [ATP], which are available in the literature. Unlike V and D, $\dot{Q}$ is not immediately accessible from the time traces of the motor. However, as long as the kinetic network model is physically sensible enough to correctly describe the transport dynamics of the motor, the rate constants $\{k_{ij}\}$ determined by fitting the data of $V(\{k_{ij}(f, [\mathrm{ATP}])\})$ and $D(\{k_{ij}(f, [\mathrm{ATP}])\})$ to the network model allow us to calculate $\dot{Q}(\{k_{ij}(f, [\mathrm{ATP}])\})$[22] and, hence $\mathcal{Q}(f, [\mathrm{ATP}])$. Projection of molecular processes in a low-dimensional space is reasonable approximation as long as there exists a time scale separation between a slow variable of interest and other faster variables.[23] Because a series of chemical transformations involving ATP binding and hydrolysis followed by P_i and ADP release from the motor head domain are the slowest events in the motor dynamics, representing the time trajectories of molecular motors onto the chemical state space is deemed a good approximation.

For kinesin-1, we employ the motility data analyzed in terms of $V(f, [\mathrm{ATP}])$ and $D(f, [\mathrm{ATP}])$ from ref 24 (Figure S1) and model them using the six-state kinetic network model[25] consisting of two cycles $\mathcal{F}$ and $\mathcal{B}$ (Figure 1A). Although the conventional (N = 4)-state unicyclic model[26,27] confers a similar result with the double-cycle model at small f (compare Figures 1 and S3), the unicyclic model leads to a physically problematic interpretation especially when the molecular motor is stalled or starts taking backsteps at large hindering load.[25,28,29] As explicated previously,[29] the backstep in the unicyclic network, by construction, is produced by a reversal of the forward cycle, which implies that the backstep is always realized via the synthesis of ATP from ADP and P_i. More importantly, the unicyclic network results in $\dot{Q} = 0$ under the stall condition, which however contradicts the physical reality; an idling car still burns fuel and dissipates heat ($\dot{Q} \neq 0$)! To accommodate the possibility of an ATP-induced (fuel-burning) backstep or ATP-consuming stall into our consideration, we extend the unicyclic network into a multicyclic one.[25,29−31]

The proposed double-cycle network is a minimal reaction network model that can accommodate four different scenarios for the kinetic paths: (i) ATP hydrolysis-induced forward step; (ii) ATP hydrolysis-induced backward step; (iii) ATP synthesis-induced forward step; (iv) ATP synthesis-induced backward step. With the rate constants determined against the motility data of kinesin-1 using the double-cycle model, the kinesin-1 predominantly moves forward through the $\mathcal{F}$ cycle under small hindering ($f \gtrsim 0$) or assisting load ($f < 0$), whereas it takes a backstep through the $\mathcal{B}$ cycle under a large hindering load. In principle, the reaction current within the $\mathcal{F}$ cycle ($J_{\mathcal{F}}$) is decomposed into the forward ($J_{\mathcal{F}}^{+}$) and backward current

DOI: 10.1021/acs.jpclett.7b03197
J. Phys. Chem. Lett. 2018, 9, 513−520

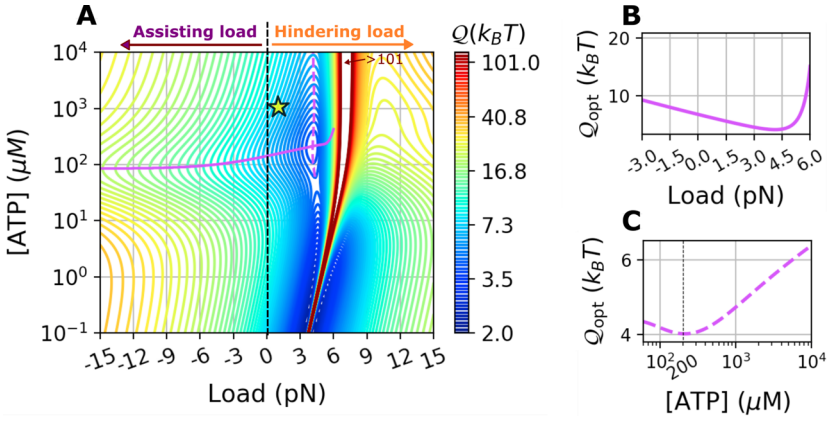

Figure 2. $\mathcal{Q}$ calculated based on kinesin-1 data[24] using the six-state double-cycle model[25] at varying f and [ATP], where $f > 0$ and $f < 0$ stand for the hindering and assisting load, respectively. (A) 2-D contour plot of $\mathcal{Q} = \mathcal{Q}(f, [\mathrm{ATP}])$. A suboptimal point $\mathcal{Q}_{\mathrm{opt}} \approx 4k_{\mathrm{B}}T$ is found at $f = 4.1$ pN and [ATP] ≈ 210 μM. The solid lines in magenta are the loci of locally optimal $\mathcal{Q}$ at varying [ATP] for a given f (B). The dashed lines in magenta are the loci of locally optimal $\mathcal{Q}$ at varying f for a given [ATP] (C). The star symbol indicates the cellular condition of [ATP] ≈ 1 mM and $f \approx 1$ pN.

$(J_{\mathcal{F}}^{-})$, satisfying $J_{\mathcal{F}} = J_{\mathcal{F}}^{+} - J_{\mathcal{F}}^{-} > 0$. Although a backstep satisfying $J_{\mathcal{F}} < 0$ could be realized through an ATP synthesis,[32] a theoretical analysis[29] on the experimental data[33,34] suggests that such a backstep current ($J_{\mathcal{F}} < 0$, ATP synthesis-induced backstep) is practically negligible compared with the current associated with an ATP hydrolysis-induced backstep ($J_{\mathcal{B}} > 0$), so that $|J_{\mathcal{B}}| \gg |J_{\mathcal{F}}|$.

We demonstrate the dynamics of kinesin-1 realized in the double-cycle network in terms of $J_{\mathcal{F}}$ and $J_{\mathcal{B}}$ with increasing f (see Figure 1B). At $f = 0$, kinesin-1 predominantly moves forward ($J_{\mathcal{F}} \gg J_{\mathcal{B}}$). This imbalance diminishes as f increases until it reaches $f = f_{\mathrm{stall}}$. At stall conditions, the net current J associated with the mechanical stepping defined between states (2) and (5) vanishes ($J = J_{\mathcal{F}} - J_{\mathcal{B}} = 0$); however, non-vanishing current due to ATP chemistry still persists along the path of → (2) → (3) → (4) → (5) → (6) → (1) → (2) → (see Figure 1A). A further increase of f beyond f_{stall} renders $J_{\mathcal{F}} < J_{\mathcal{B}}$, augmenting the likelihood of backstep.

We also demonstrate the rates of heat dissipation ($\dot{Q}$), work production ($\dot{W}$), and total energy supply ($\dot{E}$). In the double-cyclic model, the total heat generated from the kinetic cycle depicted in Figure 1A is decomposed into two contributions from the subcycles, $\dot{Q}_{\mathcal{F}}$ and $\dot{Q}_{\mathcal{B}}$, each of which is the product of reaction current and affinity[8,25,35−38]

$$\dot{Q} = \dot{Q}_{\mathcal{F}} + \dot{Q}_{\mathcal{B}} = J_{\mathcal{F}}\mathcal{A}_{\mathcal{F}} + J_{\mathcal{B}}\mathcal{A}_{\mathcal{B}} \tag{3}$$

Here, the affinities (driving forces) for the $\mathcal{F}$ and $\mathcal{B}$ cycles are

$$\mathcal{A}_{\mathcal{F}} = k_{\mathrm{B}}T \log\left(\frac{k_{12}k_{25}k_{56}k_{61}}{k_{21}k_{16}k_{65}k_{52}}\right) = (-\Delta\mu_{\mathrm{hyd}}) - fd_0 \tag{4}$$

and

$$\mathcal{A}_{\mathcal{B}} = k_{\mathrm{B}}T \log\left(\frac{k_{23}k_{34}k_{45}k_{51}}{k_{32}k_{25}k_{54}k_{43}}\right) = (-\Delta\mu_{\mathrm{hyd}}) + fd_0 \tag{5}$$

The expressions of $J_{\mathcal{F}}$ and $J_{\mathcal{B}}$ in terms of $\{k_{ij}\}$ are available (see eq S25), but they are generally more complicated than that of affinity. The above decomposition of the affinity associated with each cycle into the chemical driving force and the work done by the motor straightforwardly follows from the expression of $\{k_{ij}\}$ (see the Methods Section for the expressions of f-dependent rate constants).[25−27] From eqs 3−5, $\dot{Q}$ can be decomposed into the total free energy input ($\dot{E} = (J_{\mathcal{F}} + J_{\mathcal{B}})(-\Delta\mu_{\mathrm{hyd}})$) and work production ($\dot{W} = (J_{\mathcal{F}} - J_{\mathcal{B}})fd_0$)

$$\dot{Q} = (J_{\mathcal{F}} + J_{\mathcal{B}})(-\Delta\mu_{\mathrm{hyd}}) - (J_{\mathcal{F}} - J_{\mathcal{B}})fd_0 = \dot{E} - \dot{W} \tag{6}$$

A few points are noteworthy from the dependences of V, D, $\dot{Q}$, and $\dot{W}$ on f and [ATP] (see Figure 1): (i) The stall condition, depicted by a white dashed line in each map, divides all of the 2D diagrams of V, D, $\dot{Q}$, and $\dot{W}$ into two regions; (ii) $\dot{Q}$ and $\dot{W}$ display nonmonotonic dependences on f (Figure 1F,G); at high [ATP] (∼2 mM), $\dot{Q}$ is locally maximized at $f =$ 10 pN, whereas $\dot{W}$ is maximized at 5 pN and locally minimized at 10 pN (see Figure 1I calculated at [ATP] = 2 mM); (iii) at $f = f_{\mathrm{stall}}$ (∼7 pN) (Figures 1B,I, black dashed line), the reaction current of the $\mathcal{F}$ cycle is exactly balanced with that of the $\mathcal{B}$ cycle ($J = J_{\mathcal{F}} - J_{\mathcal{B}} = 0$), giving rise to zero work production ($\dot{W} = fV = fd_0J = 0$). The numbers of forward and backward steps taken by the motor are identical, and hence, there is no net directional movement ($V = 0$).[34] Importantly, even at the stall condition, kinesin-1 hydrolyzes ATP, dissipating heat in both forward and backward steps and, hence, rendering $\dot{Q} = (J_{\mathcal{F}} + J_{\mathcal{B}})(-\Delta\mu_{\mathrm{hyd}})$ always positive.

Quantification of $\mathcal{Q}$ for Kinesin-1. Unlike V, D, and $\dot{Q}$, which are maximized at large [ATP] and small f (Figure 1D−F), $\mathcal{Q}(f, [\mathrm{ATP}])$ displays a complex functional dependence (Figure 2A). (i) $\mathcal{Q} \to 2k_{\mathrm{B}}T$ at low [ATP] and f. However, this is a trivial outcome of the detailed balance condition where [ATP] is balanced with [ADP] and [P_i]. The motor, without a chemical driving force and only subjected to thermal fluctuations ($\dot{Q} \to 0$), is, on average, motionless ($V \to 0$) but with a finite dispersion ($D \neq 0$); $\mathcal{Q}$ is minimized in this case ($\mathcal{Q} \to 2k_{\mathrm{B}}T$) (see eq 2). (ii) $\mathcal{Q}$ is generally smaller below the stall condition, $f < f_{\mathrm{stall}}([\mathrm{ATP}])$, demarcated by the white dashed lines in Figure 1. In this case, the reaction current along the $\mathcal{F}$ cycle is more dominant than that above the stall. At the stall, $\mathcal{Q}$ diverges because of $V \to 0$ and $\dot{Q} \neq 0$ (eq 2). (iii) Notably, a suboptimal value of $\mathcal{Q} \approx 4k_{\mathrm{B}}T$ is identified at [ATP] = 210 μM and $f = 4.1$ pN (Figures 2). (iv) At $f \approx 4$ pN, the

DOI: 10.1021/acs.jpclett.7b03197
J. Phys. Chem. Lett. 2018, 9, 513−520

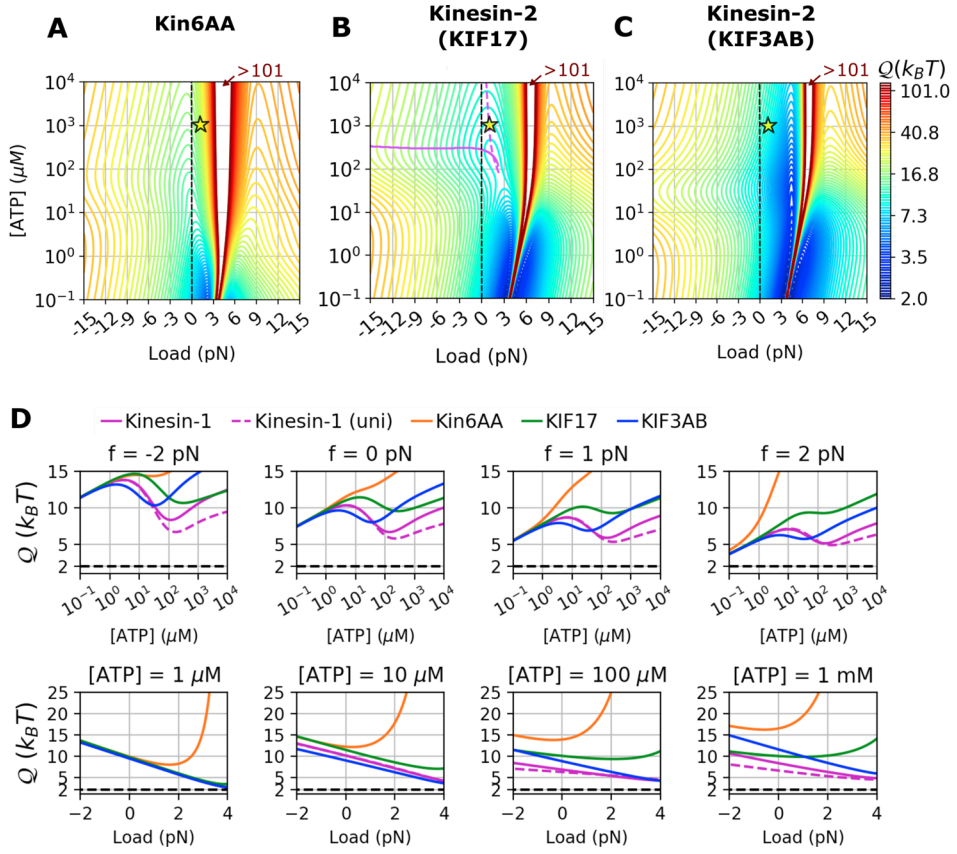

Figure 3. $Q(f, [\mathrm{ATP}])$ calculated for (A) Kin6AA,[31] (B) homodimeric kinesin-2 KIF17,[45] and (C) heterotrimeric kinesin-2 KIF3AB.[45] In (A–C), the condition of $[\mathrm{ATP}] \approx 1$ mM and $f \approx 1$ pN is indicated with the star symbols. (D) $Q([\mathrm{ATP}])$ at fixed f (upper panels) and $Q(f)$ at fixed [ATP] (lower panels) calculated for kinesin-1 (solid magenta lines for the six-state network model and dashed magenta lines for the unicyclic model), Kin6AA (orange lines), KIF17 (green lines), and KIF3AB (blue lines). The black dashed lines depict $Q = 2k_BT$.

transport efficiency of kinesin-1 ($4k_BT \lesssim Q \lesssim 6k_BT$) remains unchanged over the broad range of [ATP] (= 1 μM − 10 mM) (Figure 2C).

Comparison between Different Types of Kinesins. The dynamic property of the molecular motor differs from one motor type to another. The effect of modifying the motor structure on the transport properties as well as on the directionality and processivity of the molecular motor has been of great interest because it provides understanding into the design principle of a motor at the microscopic level.[39−43] To address how modifications to the motor structure alter the transport efficiency, we analyze single-molecule motility data of a mutant of kinesin-1 (Kin6AA) and homodimeric and heterotrimeric kinesin-2 (KIF17 and KIF3AB).

Data of Kin6AA, a mutant of kinesin-1 that has a six-residue longer neck-linker domain, were taken from ref 31. Insertion of six amino acid residues into the neck-linker reduces the internal tension along the neck-linker, which disturbs chemical coordination between the two motor heads[44] and impairs the motility of the motor. We analyzed the data of Kin6AA again using the six-state network model (Figures 1A, S4, and S5 and Table S2; see the Supporting Information for detail), indeed finding reductions of V, D (Figure S5A), and $f_{\mathrm{stall}}([\mathrm{ATP}])$ (Figure S5A, white dashed line). Of particular note is that the rate constant k_{2S} associated with the physical step is reduced by 2 orders of magnitude (Table S2). In $Q(f, [\mathrm{ATP}])$ (Figure 3A), the suboptimal point observed in the wild-type (Figure 2A) vanishes (Figure 3A), and the decreased stall force makes Q diverge at smaller force (~4 pN). Overall, there is a dramatic increase in Q, indicating that the trajectory of Kin6AA is less regular and unpredictable ($Q \approx 20k_BT$) than that of kinesin-1 ($Q \approx 7k_BT$). Thus, Kin6AA is less efficient than the wild-type in cargo transport.

Next, the values of Q were calculated for two active forms of vertebrate kinesin-2 class motors responsible for intraflagellar transport (IFT). KIF17 is a homodimeric form of kinesin-2, and KIF3AB is a heterotrimeric form made of KIF3A, KIF3B, and a nonmotor accessory protein, KAP. To quantify their motility properties, we digitized single-molecule motility data from ref 45 and analyzed them again using the six-state double-cycle model (Figures S6 and S8). $Q(f, [\mathrm{ATP}])$ values of KIF17 and KIF3AB are qualitatively similar to that of kinesin-1 with some variations. Q for KIF17 forms a shallow local minimum of $Q \approx 9.2k_BT$ at [ATP] = 200 μM and f = 1.5 pN (Figure 3B), whereas such a suboptimal condition is less clear in KIF3AB (Figure 3C). Instead, KIF3AB displays a local valley of Q at around $f \approx 4$ pN and 1 μM $\lesssim$ [ATP] $\lesssim$ 10 mM in which $Q \approx 4k_BT$.

The plots of $Q([\mathrm{ATP}])$ at fixed f and $Q(f)$ with fixed [ATP] in Figure 3D recapitulate the difference between different classes of kinesins more clearly. (i) An extension of the neck-linker domain (Kin6AA, orange lines) dramatically increases Q compared with the wild-type (Kinesin WT, magenta lines). (ii) Nonmonotonic behaviors of $Q([\mathrm{ATP}])$ are qualitatively similar for all kinesin types. (iii) The movement of KIF3AB (blue

DOI: 10.1021/acs.jpclett.7b03197
J. Phys. Chem. Lett. 2018, 9, 513−520

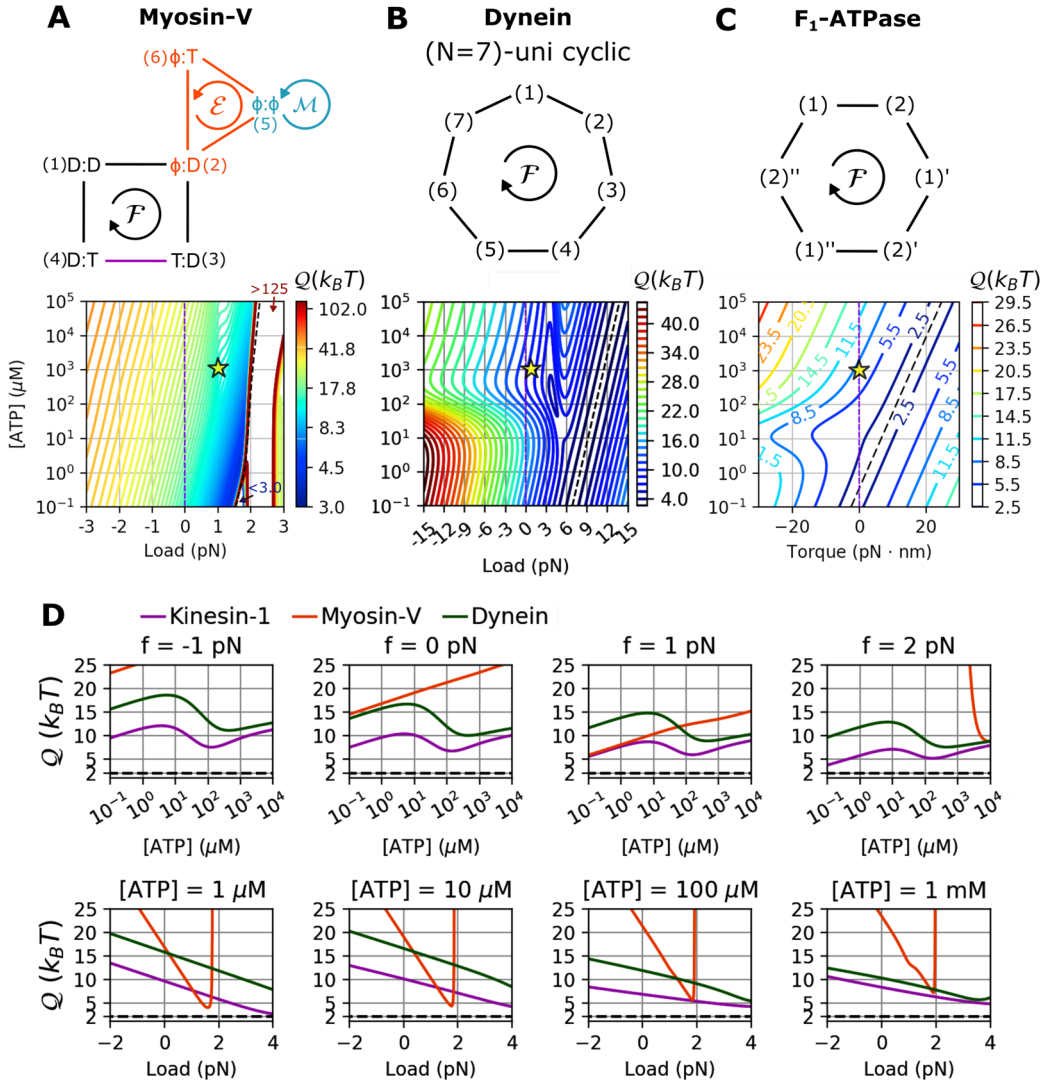

Figure 4. $\mathcal{Q}(f, [\mathrm{ATP}])$ for various motors. (A) Kinetic model for myosin-V consisting of three cycles $\mathcal{F}$, $\mathcal{E}$, and $\mathcal{M}$.[46] $\mathcal{Q}(f, [\mathrm{ATP}])$ calculated at $[\mathrm{ADP}] = 70\ \mu\mathrm{M}$ and $[\mathrm{P_i}] = 1$ mM (see also Figure S11D for a 2-D heat map). (B) ($N = 7$)-unicyclic kinetic model for cytoplasmic dynein and the corresponding $\mathcal{Q}(f, [\mathrm{ATP}])$ calculated based on the kinetic parameters provided in ref 47 at $[\mathrm{ADP}] = 70\ \mu\mathrm{M}$ and $[\mathrm{P_i}] = 1$ mM (see also Figure S13D for a 2-D heat map). (C) $\mathcal{Q}(f, [\mathrm{ATP}])$ at $[\mathrm{ADP}] = 70\ \mu\mathrm{M}$ and $[\mathrm{P_i}] = 1$ mM (see also Figure S13D for a 2-D heat map) using the kinetic model for F_1-ATPase from ref 48. Other quantities such as V, D, and $\mathcal{A}$ as a function of f and [ATP] are provided in Figures S11, S13, S14. (D) $\mathcal{Q}([\mathrm{ATP}])$ at fixed f (upper panels) and $\mathcal{Q}(f)$ at fixed [ATP] (lower panels) for kinesin-1 (magenta), myosin-V (orange), and dynein (green).

lines) becomes the most regular at low [ATP] ($\lesssim$10 μM). (iv) $\mathcal{Q}$ for kinesin-1 analyzed using the (N = 4)-state unicyclic model (dashed magenta lines) displays only small deviations as long as $0 \lesssim f \lesssim 4 \ll f_{\mathrm{stall}} \approx 7$ pN. The observation in (iv) implies that in the parameter range of f and [ATP] where V and D can be fitted well by a selected model $\mathcal{Q}$ remains largely invariant with the choice of model. Further, $\mathcal{Q}(f, [\mathrm{ATP}])$ values do not show significant difference as long as $f < f_{\mathrm{st}}$ (see Figures 3D, 2A, and S3D and Table S1).

Comparison of $\mathcal{Q}$ among Different Types of Motors. We further investigate $\mathcal{Q}(f, [\mathrm{ATP}])$ for other motor types, myosin-V, dynein, and F_1-ATPase, using the kinetic network models and the corresponding rate constants proposed in the literature.[46−48] The details of the kinetic model for each motor and rate constants are provided in the Supporting Information.

Myosin-V: The model studied in ref 46 consists of a chemomechanical forward cycle $\mathcal{F}$, dissipative cycle $\mathcal{E}$, and pure mechanical cycle $\mathcal{M}$ (Figure 4A). In the $\mathcal{F}$ cycle, myosin-V either moves forward by hydrolyzing ATP or takes a backstep via ATP synthesis. In the $\mathcal{M}$ cycle, myosin-V moves backward under the load without involving chemical reactions. The $\mathcal{E}$ cycle places a bridge between the two cycles $\mathcal{F}$ and $\mathcal{M}$. No local minimum is found in $\mathcal{Q}(f, [\mathrm{ATP}])$ when it is calculated at $[\mathrm{ADP}] = 70\ \mu\mathrm{M}$ and $[\mathrm{P_i}] = 1$ mM using the rate constants from ref 46 (see Figure S11). However, at $[\mathrm{ADP}] = 0.1\ \mu\mathrm{M}$ and $[\mathrm{P_i}] = 0.1\ \mu\mathrm{M}$, which is the condition used in ref 46, a local minimum with $\mathcal{Q} = 6.5 k_B T$ is identified at $f = 1.1$ pN and $[\mathrm{ATP}] = 20\ \mu\mathrm{M}$ (Figure S12D, Table S1). In the (N = 2)-unicyclic model for myosin-V (Figure S15),[49] $\mathcal{Q}$ has local valley at around $f \approx 2$ pN and $[\mathrm{ATP}] \approx 10\ \mu\mathrm{M}$.

Dynein: $\mathcal{Q}(f, [\mathrm{ATP}])$ for cytoplasmic dyneins was evaluated using the (N = 7)-unicyclic model (Figure 4B) and parameters used in a previous study.[47] $\mathcal{Q}(f, [\mathrm{ATP}])$ calculated from the model is locally minimized to $\mathcal{Q} \approx 5.2 k_B T$ at $f = 3.9$ pN, $[\mathrm{ATP}] = 200\ \mu\mathrm{M}$ (Figures 4D and S13D), the condition of which is

DOI: 10.1021/acs.jpclett.7b03197
J. Phys. Chem. Lett. 2018, 9, 513−520

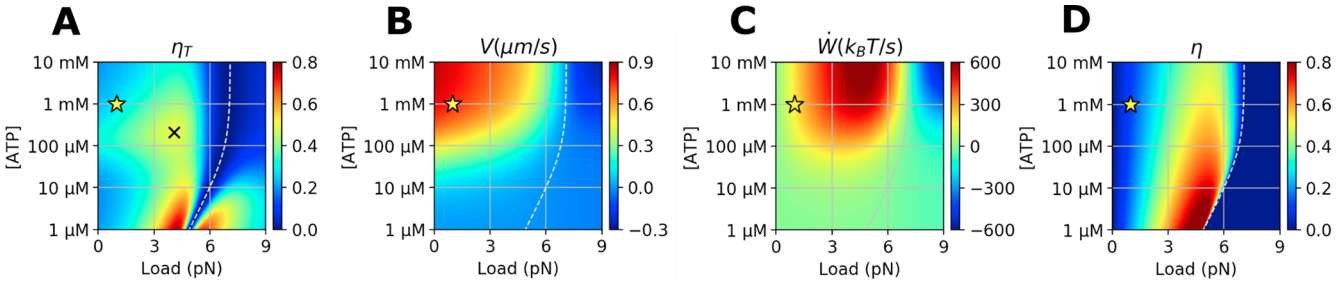

Figure 5. Various quantities calculated for kinesin-1 at varying conditions of f and [ATP]. (A) Transport efficiency η_T($= 2k_BT/Q$). A suboptimal point $\eta_T^* \approx 0.48$ (indicated by the symbol ×) is formed at $f = 4.1$ pN and [ATP] = 210 μM. (B) Transport speed $V(f, [ATP])$, (C) work production $\dot{W}(f, [ATP])$, and (D) power efficiency calculated using $\eta \equiv \dot{W}/\dot{E}$. For $f > f_{stall}$, we set $\eta = 0$ for convenience because the motor moves backward and $\dot{W} < 0$. At the cellular condition ($f \approx 1$ pN and [ATP] ≈ 1 mM), indicated by the star symbol in each panel, $\eta_T = 0.28$, $V = 0.74$ μm/s, $\dot{W} = 182k_BT/s$, and $\eta = 0.12$.

compatible with the local minimum of $Q_{kinesin\text{-}1}(f, [ATP])$ (Table S1).

F_1-ATPase: F_1-ATPase is a rotary molecular motor. In vivo, it combines with the F_0 subunit and synthesizes ATP by using a proton gradient across the membrane. $Q(\tau, [ATP])$ calculated using the ($N = 2$)-state unicyclic model in ref 48 (also see the Supporting Information for the detailed model description) reveals that there is a valley at around torque $\tau \approx -10$ pN·nm and [ATP] ≈ 10 μM, reaching $Q \approx 4k_BT$ (Figure 4C). Notably, Q for F_1-ATPase is optimized at the hindering load ($\tau < 0$) in which ATP is synthesized, which comports well with the biologically known role of F_1-ATPase as an ATP synthase in vivo.

To highlight the difference between the motors, we plot $Q([ATP])$ at fixed f and $Q(f)$ at fixed [ATP] in Figure 4D, which finds $Q_{kinesin\text{-}1} < Q_{dynein} < Q_{myosin\text{-}V}$ over the broad range of f and [ATP]. We note that at a special condition ([ATP] = 1−10 μM and f = 1−2 pN) $Q_{myosin\text{-}V}$ is smaller than the values of other motors.

We have quantified the uncertainty measure Q for various biological motors, finding that $Q(f, [ATP])$ values for motors are semioptimized near the cellular condition (star symbols marking $f \approx 1$ pN and [ATP] = 1 mM in Figures 2−4). The value of Q/k_BT calculated under the cellular condition increases in the following order: 7.2 (kinesin-1) < 7.7 (F_1-ATPase) < 9.1 (dynein) < 9.9 (KIF17, KIF3AB) < 13 (myosin-V) < 19 (Kin6AA). Among the molecular motors studied here, kinesin-1 is the best motor whose Q ($\sim 7.2k_BT$) is the closest to the theoretical bound ($Q = 2k_BT$), whereas Kin6AA has the worst efficiency with $Q \approx 19k_BT$, significantly greater than the value for the wild-type.

Minimizing Q toward its lower bound $2k_BT$ is equivalent to maximizing the transport efficiency, which can be defined to range between 0 and 1 as[21]

$$\eta_T(f, [ATP]) = \frac{2k_BT}{Q(f, [ATP])} \tag{7}$$

The structure of $\eta_T(f, [ATP])$ (equivalently $Q(f, [ATP])$) differs significantly from that of other quantities such as the flux $J(f, [ATP])$[20] (equivalent to $V(f, [ATP])$), the work production (power) $\dot{W}(f, [ATP])$, and the power efficiency $\eta(f, [ATP]) \equiv \dot{W}(f, [ATP])/\dot{E}(f, [ATP])$ (Figure 5 for kinesin-1; see the Supporting Figures for other motors). In fact, the thermodynamic uncertainty relation provides universal upper bounds on the power or the power efficiency via $\dot{Q} \geq 2k_BTV^2/D$.[50] Of particular note is that only $\eta_T(f, [ATP])$ displays a suboptimal peak (× symbol in Figure 5A) near the cellular condition.

To what extent can our findings on the-single motor efficiency in vitro be generalized to those in live cells? First, the force hindering the motor movement varies with cargo size and subcellular location; the load or viscoelastic drag exerted on motors varies dynamically.[51,52] Yet, actual forces opposing the cargo movement in a cytosolic environment are still $\lesssim$1 pN.[53,54] Because Q values for microtubule-binding motors, kinesin-1, kinesin-2, and dynein, are narrowly tuned, varying only a few k_BT over the range of $0 \leq f \leq 4$ pN at [ATP] = 1 mM (Figures 3D, 4D), our discussion can be extended to the cargo transport in a cytosolic environment as well. Next, a team of motors is often responsible for cargo transport in the cell.[55] Although trajectories generated by multiple motors have not been studied here, extension of the present analysis to such cases is straightforward. It has, however, been shown that the extent of coordination between two kinesin motors attached to cargo is insignificant under the condition of small f and saturating ATP.[56]

In the axonal transport, of particular importance is the fast and timely delivery of cellular material, the failure of which is linked to neuropathology.[57,58] Because there are already numerous regulatory mechanisms, it could be argued that the role played by the optimized single motor is redundant and plays a minor role. Yet, given that cellular regulations are realized through multiple layers of checkpoints,[4] the optimized efficiency of an individual motor can also be viewed as one of the checkpoints that ensure optimal cargo transport.

Taken together, the thermodynamic uncertainty relation, a general principle for dissipative processes in NESSs, offers quantitative insight into the energy−speed−precision trade-off relation for cargo transport by molecular motors. Given that there are many possible directions to designing the motor structure, it is significant to find that biological motors indeed possess a semioptimal transport efficiency under the cellular condition. Finally, it is of great interest to extend the concept and analysis presented here to other energy-consuming error-correcting machineries such as molecular chaperones.[59]

METHODS SECTION

Determination of Rate Constants for a Kinetic Network. To describe the kinetic transitions of kinesin-1 in the six-state double-cyclic network (Figure 1A), we used the following expressions for the rate constants: (i) Bell-like expressions,

DOI: 10.1021/acs.jpclett.7b03197
J. Phys. Chem. Lett. 2018, 9, 513−520

$k_{25}(f) = k_{25}^{o}e^{-\theta f d_0/k_BT}$ and $k_{52}(f) = k_{52}^{o}e^{-(1-\theta)f d_0/k_BT}$, for the mechanical transitions between the states (2) and (5) and (ii) $k_{ij}(f) = k_{ij}^{chem}(f) = 2k_{ij}^{o}(1 + e^{\chi_{ij} f d_0/k_BT})^{-1}$ with $\chi_{ij} = \chi_{ji} > 0$ for the other chemistry-related transitions ($k_{ij} \neq k_{25}, k_{52}$).[25] The functional form of $k_{ij}^{chem}(f)$ models the effect of motor head distortion elicited by a high external load that hinders the binding and hydrolysis of ATP in the catalytic site.[41,44,60] Note that for $f \gg f_{stall}$ $k_{ij}^{chem} \rightarrow 0$, which also leads to $\dot{Q} = 0$ (Figure 1B,F,I).

The rate constants determined for the $\mathcal{F}$ cycle were used for the corresponding chemical steps in the $\mathcal{B}$ cycle.[25] For example, the ADP dissociation rate constant k_{23} of the $\mathcal{B}$ cycle is equal to k_{56}, corresponding to the ADP dissociation step in the $\mathcal{F}$ cycle. Similarly, $k_{32} = k_{65}$, $k_{34} = k_{61}$, $k_{43} = k_{16}$, $k_{45}(= k_{45}^{bi}[ATP]) = k_{12}(= k_{12}^{bi}[ATP])$, $\chi_{23} = \chi_{56}$, $\chi_{34} = \chi_{61}$, and $\chi_{45} = \chi_{12}$. Because the ATP hydrolysis free energy that drives the $\mathcal{F}$ and $\mathcal{B}$ cycles is identical, $(k_{12}k_{25}k_{56}k_{61}/k_{21}k_{52}k_{65}k_{16}) = (k_{23}k_{34}k_{45}k_{52}/k_{32}k_{43}k_{54}k_{25})$; thus $k_{54} = k_{21}(k_{52}/k_{25})^2$.[25] Because of the paucity of data at high load condition[24] that activates the $\mathcal{B}$ cycle, it is not easy to determine all of the parameters for $\mathcal{F}$ and $\mathcal{B}$ cycles simultaneously. To circumvent this difficulty, we fitted the data using the following procedure: (i) The affinity $\mathcal{A}$ at $f = 0$ was determined from our previous study that employed the ($N = 4$)-state unicyclic model.[22] Even though the $\mathcal{B}$ cycle is not considered in ref 22, $J_{\mathcal{B}} \approx 0$ at $f \approx 0$, which justifies the use of the unicyclic model at $f \ll f_{stall}$; (ii) the range of parameters was constrained during the fitting procedure (Table S3) based on the values provided in refs 25 and 29. The `minimize` function with the "L-BFGS-B" method from the scipy library was used to fit the data globally.

The set of rate constants $k_{ij}(f, [ATP])$ determined from the fit allow us to calculate the reaction current (J), current fluctuation (δJ^2), affinity ($\mathcal{A}$, net driving force), heat dissipation ($\dot{Q}$), and, hence, $\mathcal{Q}$ (eq 2) associated with the network.

Unlike [ATP], most experiments do not investigate the effects of variation in [ADP] and [P_i] on the motility of motors. In practice, the concentrations of ADP and P_i are kept constant. Unless stated otherwise, [ADP] = 70 μM and [P_i] = 1 mM are assumed as the conditions for the experiment or cellular environment.

Details of kinetic network models and corresponding rate constants used for the analyses of other motors (Kin6AA, KIF17, KIF3AB, myosin-V, dynein, and F_1-ATPase) are provided in the Supporting Information.

■ ASSOCIATED CONTENT

Supporting Information

The Supporting Information is available free of charge on the ACS Publications website at DOI: 10.1021/acs.jpclett.7b03197.

Detailed derivation of V and D for the chemical network models of the biological motors discussed in the main text, procedure of estimating the rate constants of kinesin motors, analysis of unicyclic models for kinesin-1 and myosin-V, Figures S1−S15, showing analysis of experimental data, various physical properties, motility data, and the augmented kinetic network model of myosin-V, and Tables S1−S8, providing optimal values of f and [ATP], determined parameters, initial values and constraints, parameters used for calculations, and polynomial coefficients (PDF)

■ AUTHOR INFORMATION

Corresponding Author

*E-mail: hyeoncb@kias.re.kr.

ORCID

Changbong Hyeon: 0000-0002-4844-7237

Notes

The authors declare no competing financial interest.

■ ACKNOWLEDGMENTS

We thank Steven P. Gross for insightful comments on cargo transport in live cells. This work was performed in part at the Aspen Center for Physics, which is supported by National Science Foundation Grant PHY-1607611. We acknowledge the Center for Advanced Computation in KIAS for providing computing resources.

■ REFERENCES

(1) Hopfield, J. J. Kinetic Proofreading: A New Mechanism for Reducing Errors in Biosynthetic Processes Requiring High Specificity. *Proc. Natl. Acad. Sci. U. S. A.* **1974**, *71*, 4135−4139.

(2) Ehrenberg, M.; Blomberg, C. Thermodynamic Constraints on Kinetic Proofreading in Biosynthetic Pathways. *Biophys. J.* **1980**, *31*, 333−358.

(3) Bennett, C. H. The Thermodynamics of Computation − a Review. *Int. J. Theor. Phys.* **1982**, *21*, 905−940.

(4) Alberts, B.; Johnson, A.; Lewis, J.; Raff, M.; Roberts, K.; Walter, P. *Molecular Biology of the Cell*, 5th ed.; Garland Science, 2008.

(5) Mehta, P.; Schwab, D. J. Energetic Costs of Cellular Computation. *Proc. Natl. Acad. Sci. U. S. A.* **2012**, *109*, 17978−17982.

(6) Lan, G.; Sartori, P.; Neumann, S.; Sourjik, V.; Tu, Y. The Energy-Speed-Accuracy Trade-Off in Sensory Adaptation. *Nat. Phys.* **2012**, *8*, 422−428.

(7) Banerjee, K.; Kolomeisky, A. B.; Igoshin, O. A. Elucidating Interplay of Speed and Accuracy in Biological Error Correction. *Proc. Natl. Acad. Sci. U. S. A.* **2017**, *114*, 5183−5188.

(8) Barato, A. C.; Seifert, U. Thermodynamic Uncertainty Relation for Biomolecular Processes. *Phys. Rev. Lett.* **2015**, *114*, 158101.

(9) Gingrich, T. R.; Horowitz, J. M.; Perunov, N.; England, J. L. Dissipation Bounds All Steady-State Current Fluctuations. *Phys. Rev. Lett.* **2016**, *116*, 120601.

(10) Pietzonka, P.; Barato, A. C.; Seifert, U. Universal Bounds on Current Fluctuations. *Phys. Rev. E: Stat. Phys., Plasmas, Fluids, Relat. Interdiscip. Top.* **2016**, *93*, 052145.

(11) Pigolotti, S.; Neri, I.; Roldán, É.; Jülicher, F. Generic Properties of Stochastic Entropy Production. *Phys. Rev. Lett.* **2017**, *119*, 140604.

(12) Hyeon, C.; Hwang, W. Physical Insight into the Thermodynamic Uncertainty Relation Using Brownian Motion in Tilted Periodic Potentials. *Phys. Rev. E: Stat. Phys., Plasmas, Fluids, Relat. Interdiscip. Top.* **2017**, *96*, 012156.

(13) Proesmans, K.; Van den Broeck, C. Discrete-Time Thermodynamic-like Uncertainty Relation. *EPL* **2017**, *119*, 20001.

(14) Callen, H. B. *Thermodynamics and an Introduction to Thermostatistics*; Wiley, 1985.

(15) Curzon, F. L.; Ahlborn, B. Efficiency of a Carnot Engine at Maximum Power Ouput. *Am. J. Phys.* **1975**, *43*, 22−24.

(16) Lee, J. S.; Park, H. Carnot Efficiency is Reachable in an Irreversible Process. *Sci. Rep.* **2017**, *7*, 10725.

(17) Bustamante, C.; Keller, D.; Oster, G. The physics of molecular motors. *Acc. Chem. Res.* **2001**, *34*, 412−420.

(18) Wang, H.; Oster, G. The Stokes efficiency for molecular motors and its applications. *EPL (Europhysics Letters)* **2002**, *57*, 134.

(19) Schmiedl, T.; Seifert, U. Efficiency of molecular motors at maximum power. *EPL (Europhysics Letters)* **2008**, *83*, 30005.

(20) Brown, A. I.; Sivak, D. A. Allocating Dissipation Across a Molecular Machine Cycle to Maximize Flux. *Proc. Natl. Acad. Sci. U. S. A.* **2017**, *114*, 11057−11062.

DOI: 10.1021/acs.jpclett.7b03197
J. Phys. Chem. Lett. 2018, 9, 513−520

(21) Dechant, A.; Sasa, S.-I. Current Fluctuations and Transport Efficiency for General Langevin Systems. *arXiv preprint arXiv:1708.08653*, 2017.
(22) Hwang, W.; Hyeon, C. Quantifying the Heat Dissipation from Molecular Motor's Transport Properties in Nonequilibrium Steady States. *J. Phys. Chem. Lett.* **2017**, *8*, 250−256.
(23) Zwanzig, R. *Nonequilibrium Statistical Mechanics*; Oxford University Press: New York, 2001.
(24) Visscher, K.; Schnitzer, M. J.; Block, S. M. Single Kinesin Molecules Studied with a Molecular Force Clamp. *Nature* **1999**, *400*, 184−187.
(25) Liepelt, S.; Lipowsky, R. Kinesin's Network of Chemomechanical Motor Cycles. *Phys. Rev. Lett.* **2007**, *98*, 258102.
(26) Fisher, M. E.; Kolomeisky, A. B. The Force Exerted by a Molecular Motor. *Proc. Natl. Acad. Sci. U. S. A.* **1999**, *96*, 6597−6602.
(27) Fisher, M. E.; Kolomeisky, A. B. Simple Mechanochemistry Describes the Dynamics of Kinesin Molecules. *Proc. Natl. Acad. Sci. U. S. A.* **2001**, *98*, 7748−7753.
(28) Astumian, R. D.; Bier, M. Mechanochemical Coupling of the Motion of Molecular Motors to ATP Hydrolysis. *Biophys. J.* **1996**, *70*, 637−653.
(29) Hyeon, C.; Klumpp, S.; Onuchic, J. N. Kinesin's Backsteps under Mechanical Load. *Phys. Chem. Chem. Phys.* **2009**, *11*, 4899−4910.
(30) Yildiz, A.; Tomishige, M.; Gennerich, A.; Vale, R. D. Intramolecular Strain Coordinates Kinesin Stepping Behavior along Microtubules. *Cell* **2008**, *134*, 1030−1041.
(31) Clancy, B. E.; Behnke-Parks, W. M.; Andreasson, J. O. L.; Rosenfeld, S. S.; Block, S. M. A Universal Pathway for Kinesin Stepping. *Nat. Struct. Mol. Biol.* **2011**, *18*, 1020−1027.
(32) Hackney, D. D. The Tethered Motor Domain of a Kinesin-Microtubule Complex Catalyzes Reversible Synthesis of Bound ATP. *Proc. Natl. Acad. Sci. U. S. A.* **2005**, *102*, 18338−18343.
(33) Nishiyama, M.; Higuchi, H.; Yanagida, T. Chemomechanical Coupling of the Forward and Backward Steps of Single Kinesin Molecules. *Nat. Cell Biol.* **2002**, *4*, 790−797.
(34) Carter, N. J.; Cross, R. A. Mechanics of the Kinesin Step. *Nature* **2005**, *435*, 308−312.
(35) Seifert, U. Stochastic Thermodynamics, Fluctuation Theorems and Molecular Machines. *Rep. Prog. Phys.* **2012**, *75*, 126001.
(36) Qian, H.; Beard, D. A. Thermodynamics of Stoichiometric Biochemical Networks in Living Systems Far From Equilibrium. *Biophys. Chem.* **2005**, *114*, 213−220.
(37) Qian, H. Motor Protein with Nonequilibrium Potential: Its Thermodynamics and Efficiency. *Phys. Rev. E* **2004**, *69*, 012901.
(38) Ge, H.; Qian, H. Physical Origin of Entropy Production, Free Energy Dissipation, and Their Mathematical Representation. *Phys. Rev. E* **2010**, *81*, 051133.
(39) Liao, J.-C.; Elting, M. W.; Delp, S. L.; Spudich, J. A.; Bryant, Z. Engineered Myosin VI Motors Reveal Minimal Structural Determinants of Directionality and Processivity. *J. Mol. Biol.* **2009**, *392*, 862−867.
(40) Bryant, Z.; Altman, D.; Spudich, J. A. The Power Stroke of Myosin VI and the Basis of Reverse Directionality. *Proc. Natl. Acad. Sci. U. S. A.* **2007**, *104*, 772−777.
(41) Hyeon, C.; Onuchic, J. N. A Structural Perspective on the Dynamics of Kinesin Motors. *Biophys. J.* **2011**, *101*, 2749−2759.
(42) Jana, B.; Hyeon, C.; Onuchic, J. N. The Origin of Minus-End Directionality and Mechanochemistry of Ncd Motors. *PLoS Comput. Biol.* **2012**, *8*, e1002783.
(43) Hinczewski, M.; Tehver, R.; Thirumalai, D. Design Principles Governing the Motility of Myosin V. *Proc. Natl. Acad. Sci. U. S. A.* **2013**, *110*, E4059−E4068.
(44) Hyeon, C.; Onuchic, J. N. Internal Strain Regulates the Nucleotide Binding Site of the Kinesin Leading Head. *Proc. Natl. Acad. Sci. U. S. A.* **2007**, *104*, 2175−2180.
(45) Milic, B.; Andreasson, J. O. L.; Hogan, D. W.; Block, S. M. Intraflagellar Transport Velocity is Governed by the Number of Active KIF17 and KIF3AB Motors and Their Motility Properties under Load. *Proc. Natl. Acad. Sci. U. S. A.* **2017**, *114*, E6830−E6838.
(46) Bierbaum, V.; Lipowsky, R. Chemomechanical Coupling and Motor Cycles of Myosin V. *Biophys. J.* **2011**, *100*, 1747−1755.
(47) Šarlah, A.; Vilfan, A. The Winch Model Can Explain both Coordinated and Uncoordinated Stepping of Cytoplasmic Dynein. *Biophys. J.* **2014**, *107*, 662−671.
(48) Gerritsma, E.; Gaspard, P. Chemomechanical Coupling and Stochastic Thermodynamics of the F1-ATPase Molecular Motor with an Applied External Torque. *Biophys. Rev. Lett.* **2010**, *05*, 163−208.
(49) Kolomeisky, A. B.; Fisher, M. E. A Simple Kinetic Model Describes the Processivity of Myosin-V. *Biophys. J.* **2003**, *84*, 1642−1650.
(50) Pietzonka, P.; Barato, A. C.; Seifert, U. Universal bound on the efficiency of molecular motors. *J. Stat. Mech.: Theory Exp.* **2016**, *2016*, 124004.
(51) Narayanareddy, B. R. J.; Vartiainen, S.; Hariri, N.; O'Dowd, D. K.; Gross, S. P. A Biophysical Analysis of Mitochondrial Movement: Differences Between Transport in Neuronal Cell Bodies Versus Processes. *Traffic* **2014**, *15*, 762−771.
(52) Wortman, J. C.; Shrestha, U. M.; Barry, D. M.; Garcia, M. L.; Gross, S. P.; Yu, C. C. Axonal Transport: How High Microtubule Density Can Compensate for Boundary Effects in Small-Caliber Axons. *Biophys. J.* **2014**, *106*, 813−823.
(53) Welte, M. A.; Gross, S. P.; Postner, M.; Block, S. M.; Wieschaus, E. F. Developmental Regulation of Vesicle Transport in Drosophila Embryos: Forces and Kinetics. *Cell* **1998**, *92*, 547−557.
(54) Shubeita, G. T.; Tran, S. L.; Xu, J.; Vershinin, M.; Cermelli, S.; Cotton, S. L.; Welte, M. A.; Gross, S. P. Consequences of Motor Copy Number on the Intracellular Transport of Kinesin-1-Driven Lipid Droplets. *Cell* **2008**, *135*, 1098−1107.
(55) Li, Q.; King, S. J.; Gopinathan, A.; Xu, J. Quantitative Determination of the Probability of Multiple-Motor Transport in Bead-Based Assays. *Biophys. J.* **2016**, *110*, 2720−2728.
(56) Carter, B. C.; Vershinin, M.; Gross, S. P. A Comparison of Step-Detection Methods: How Well Can You Do? *Biophys. J.* **2008**, *94*, 306−319.
(57) Mandelkow, E.; Mandelkow, E.-M. Kinesin Motors and Disease. *Trends Cell Biol.* **2002**, *12*, 585−591.
(58) Hafezparast, M.; Klocke, R.; Ruhrberg, C.; et al. Mutations in Dynein Link Motor Neuron Degeneration to Defects in Retrograde Transport. *Science* **2003**, *300*, 808−812.
(59) Chakrabarti, S.; Hyeon, C.; Ye, X.; Lorimer, G.; Thirumalai, D. Molecular Chaperones Maximize the Native State Yield on Biological Times by Driving Substrates out of Equilibrium. *Proc. Natl. Acad. Sci. U. S. A.* **2017**, *114*, E10919−E10927.
(60) Uemura, S.; Ishiwata, S. Loading Direction Regulates the Affinity of ADP for Kinesin. *Nat. Struct. Mol. Biol.* **2003**, *10*, 308−311.

DOI: 10.1021/acs.jpclett.7b03197
J. Phys. Chem. Lett. 2018, 9, 513−520